ARMY RESEARCH LABORATORY

Processing, Packaging, and Characterization of Electroceramic Materials for Phased Array Antennas

L. C. Sengupta, E. Ngo, S. Stowell, M. E. O'Day,
and R. Lancto

ARL-TR-448

May 1994

The findings in this report are not to be construed as an official Department of the Army position unless so designated by other authorized documents.

Citation of manufacturer's or trade names does not constitute an official endorsement or approval of the use thereof.

Destroy this report when it is no longer needed. Do not return it to the originator.

REPORT DOCUMENTATION PAGE

Form Approved
OMB No. 0704-0188

1. AGENCY USE ONLY *(Leave blank)*	2. REPORT DATE	3. REPORT TYPE AND DATES COVERED
	May 1994	Final Report

4. TITLE AND SUBTITLE
Processing, Packaging, and Characterization of Electroceramic Materials for Phased Array Antennas

5. FUNDING NUMBERS

6. AUTHOR(S)
L. C. Sengupta, E. Ngo, S. Stowell,
M. E. O'Day, and R. Lancto

7. PERFORMING ORGANIZATION NAME(S) AND ADDRESS(ES)
U.S. Army Research Laboratory
Watertown, MA 02172-0001
ATTN: AMSRL-MA-CA

8. PERFORMING ORGANIZATION REPORT NUMBER
ARL-TR-448

9. SPONSORING/MONITORING AGENCY NAME(S) AND ADDRESS(ES)
U.S. Army Research Laboratory
2800 Powder Mill Road
Adelphi, MD 20783-1197

10. SPONSORING/MONITORING AGENCY REPORT NUMBER

11. SUPPLEMENTARY NOTES

12a. DISTRIBUTION/AVAILABILITY STATEMENT
Approved for public release; distribution unlimited.

12b. DISTRIBUTION CODE

13. ABSTRACT *(Maximum 200 words)*

As a part of an effort to optimize the electronic device performance in the ceramic phase shifter, various composites of BSTO combined with other nonelectrically active oxide ceramics have been formulated. In general, the composites have reduced dielectric constants and loss tangents and have high tunabilities, which reduce the overall impedance mismatch and the insertion loss of the device. The combination of electronic properties of these materials offer substantially higher operating frequencies, 10 GHz and above. Grain size and phase analysis have been examined using SEM and X-ray diffraction. The packaging of the phase shifter materials electroding materials, electrode shapes, and encapsulation materials will be discussed.

14. SUBJECT TERMS	15. NUMBER OF PAGES
Barium strontium titanate	22
	16. PRICE CODE

17. SECURITY CLASSIFICATION OF REPORT	18. SECURITY CLASSIFICATION OF THIS PAGE	19. SECURITY CLASSIFICATION OF ABSTRACT	20. LIMITATION OF ABSTRACT
Unclassified	Unclassified	Unclassified	UL

Contents

Figures

Tables

1. INTRODUCTION

Phased array antennas can steer transmitted or received signals either linearly or in two dimensions without mechanically oscillating the antenna. These antennas are currently constructed using ferrite phase shifting elements. Due to the type of circuit requirements necessary to operate these antennas, they are costly, large and heavy. Therefore, the use of these antennas has been limited primarily to military applications which are strategically dependent on such capabilities. In order to make these devices available for many other commercial and military uses, the basic concept of the antenna must be improved. If ferroelectric materials could be used instead of ferrites, phased array antennas would be totally revolutionized.

A ceramic Barium Strontium Titanate, $Ba_{1-x}Sr_xTiO_3$, (BSTO), electro-optic phase shifter using a planar microstrip construction has been demonstrated[1]. In order to meet the required performance specifications, maximum phase shifting ability, the electronic properties in the low frequency (KHz) and microwave regions (GHz) must be optimized. As part of this optimization process, various composites of BSTO and non-ferroelectric oxides have been formulated. The BSTO-Alumina composite has a patent pending on its formulations and the other composites which are designated herein as BSTO-Oxide II and BSTO-Oxide III currently have a patent undergoing the filing process. All of these composites possess improved electronic properties. The comparison of the compositions and phase formation of the various BSTO-oxide ceramic composites will be made and related to their electronic properties. This report will outline some of the initial findings and compare them to the results found for pure BSTO. Also various metallizations and encapsulants have been tried and the electronic data for 20 wt% alumina, oxide II and oxide III - BSTO composites will be presented.

2. EXPERIMENTAL

2.1 Ceramic Processing

Powder forms of Barium Titanate and Strontium Titanate were obtained from Ferro Corporation, Transelco Division, Pen Yan, N.Y. (product nos. 219-6 and 218 respectively), stoichiometrically mixed to achieve $Ba_{.6}Sr_{.4}TiO_3$ and ball-milled in ethanol using 3/16" alumina media for 24 hrs. The resulting BSTO was then air-dried, calcined at 1100^{0}C and mixed with either powder alumina (ALCOA Industrial Chemicals, Bauxite, AR, distributed by Whittaker, Clark, and Daniels, South Plainfield, N.J., product no. A16-SG) or a second oxide (oxide II) or a third oxide (oxide III) in the proper weight percent and ball-milled again in a slurry of ethanol using the alumina grinding media for an addtional 24 hrs.

Three wt% of Rholpex B-60A (Rohm and Haas Co., Philadephia, PA) binder is added to the resulting BSTO/oxide mixture. The mixture is then air-dried and dry-pressed uniaxially to a pressure of approximately 7000 p.s.i.. Sintering schedules were obtained by employing a deflectometer such as Mitutoyo digimatic indicator and miniprocessor (Mitutoyo Corp., Paramus N.J.). The densities, % Porosity and % Absorption are

given in Table I. Results were obtained by performing an immersion density in ethanol using a modified ASTM standard. It should be noted that all of the examined samples have liquid absorption of less than 2%.

Two metallization techniques were employed. One involved painting two circular, aligned electrodes, one on either side of the specimens, using high purity silver paint (SPI Supplies West Chester, PA) and attaching wires using high purity silver epoxy, (Magnobond 8000, made by Magnolia Plastics, Inc., Charnblee, GA. The other technique utilized the screen printing of electrodes using silver conductive ink (FERRO #3350, Electronic Materials Division, Santa Barbara, CA) and wires were attached by dipping the specimens in a bath of 2% silver, 62% tin and 36% lead solder.

2.2 Electronic Measurements

The dielectric constants, ε', loss tan δ, % tunability were determined for all composites. The dielectric constant, ε', is derived from the complex function:

$$\varepsilon = \varepsilon' - i\varepsilon'' \quad (1)$$

The loss tan δ can be defined as:

$$\tan \delta = \varepsilon'' / \varepsilon' \quad (2)$$

and the % tunability of a material is determined using the following equation:

$$\% \text{ tunability} = \{ \varepsilon'(0) - \varepsilon'(Vapp)\} / \{\varepsilon'(0)\} \quad (3)$$

The tunability measurements were taken in an applied electric field which ranged from 0 to 3.0 V/micron (μm). The electronic properties given in the tables were measured at a frequency of 1 KHz. Capacitance measurements for all materials were taken using an HP4284A LCR meter and the dielectric constants were calculated using equation (4) and the sample dimensions.

$$\varepsilon' = Ct/A\varepsilon_0. \quad (4)$$

where

ε' = dielectric constant
C = capacitance of BSTO
t = sample thickness
A = sample area
$\varepsilon_0 = 8.8542 \times 10^{-12}$ F/m

Further calculations were done to correct for the effect of fringe capacitance. The dielectric constant has been calculated from corrected capacitance values, C_{corr}, according to equation (5). The edge (fringe) capacitance, C_e, was calculated from either equation (6) or (7) depending on the electroding configuration[2]. These equations

TABLE I Sample Descriptions of BSTO-Oxide Ceramic Composites.

BSTO-Alumina

Additive Content (wt%)	*Density (g/cc)*	*% Porosity*	*% Absorption*
0 wt% Al_2O_3	5.373	3.16	0.48
1 wt% Al_2O_3	5.319	8.94	1.43
5 wt% Al_2O_3	4.744	6.63	1.10
10 wt% Al_2O_3	4.687	7.15	1.22
20 wt% Al_2O_3	4.222	7.81	1.46
30 wt% Al_2O_3	3.965	5.05	1.03
60 wt% Al_2O_3	3.797	5.47	1.20
80 wt% Al_2O_3	3.615	7.48	1.72
pure Al_2O_3	3.992	4.44	0.95

BSTO-Oxide II

Additive Content (wt%)	*Density (g/cc)*	*% Porosity*	*% Absorption*
1 wt% Oxide II	5.22	10.31	1.64
5 wt% Oxide II	5.28	8.86	1.51
10 wt% Oxide II	5.30	7.67	1.23
15 wt% Oxide II	5.12	8.27	1.28
20 wt% Oxide II	5.37	10.31	1.64
25 wt% Oxide II	5.44	14.24	2.33
30 wt% Oxide II	5.40	9.73	1.60
40 wt% Oxide II	5.36	10.59	1.67
50 wt% Oxide II	5.22	10.34	1.70
60 wt% Oxide II	5.38	10.28	1.58

BSTO-Oxide III

Additive Content (wt%)	*Density (g/cc)*	*% Porosity*	*% Absorption*
1 wt% Oxide III	5.00	10.70	1.94
5 wt% Oxide III	5.30	3.97	0.63
10 wt% Oxide III	5.19	3.36	0.55
15 wt% Oxide III	4.95	5.38	0.97
20 wt% Oxide III	5.03	5.25	0.87
25 wt% Oxide III	4.81	3.30	0.55
30 wt% Oxide III	4.69	4.27	0.81
40 wt% Oxide III	4.42	5.40	0.98
50 wt% Oxide III	4.11	5.16	0.99
60 wt% Oxide III	3.94	2.56	0.75
80 wt% Oxide III	3.52	10.34	1.87

assume that the ground capacitance is zero and the thickness of the metal layer is much less than the thickness of the specimen.

$$C_{corr} = C_{meas} - C_e \quad (5)$$

where C_{meas} = measured capacitance value and C_e is defined below

Two cases are considered:

Both electrodes are equal but smaller than the specimen:

$$C_e = (0.0019\, C_{meas} - 0.00252 \ln t + 0.0068)\, P \quad (6)$$

Diameter of the electrodes are equal to the diameter of the specimen:

$$C_e = (0.0041\, C_{meas} - 0.0034 \ln t + 0.0122)\, P \quad (7)$$

where $P = \pi (d_{electrode} + t)$ and $d_{electrode}$ = diameter of the electrode and t = thickness of the specimen.

3. RESULTS AND DISCUSSION

3.1 SEM and EDX Analysis

SEM examination of the individual bulk ceramic layers of the BSTO-Alumina composite revealed that a secondary phase became apparent with alumina additions as low as 10 wt%. This phase becomes more dominant at 35 wt% alumina and then disappears at 60 wt%. Micrographs for these microstructures are displayed in Figs. 1(a) - 1(c). EDX of the small grains revealed a depletion in alumina while EDX of the larger, smoother grains displayed an increase in the alumina content. This suggests the formation of a barium aluminum titanium oxide phase.

SEM examination of the individual BSTO-Oxide II and BSTO-Oxide III compositions showed very little microstructural difference with added percentages of oxide. A small reduction in grain size was the most apparent difference. A micrograph of typical BSTO-Oxide II and BSTO-Oxide III microstructures are shown in Figs. 2(a) and (b). EDX analysis of the individual layers showed no unusual behavior with the percentage of oxide II or oxide III gradually increasing with steady decreases in barium, strontium and titanium.

3.2 X-Ray Diffraction

A summary of the X-Ray diffraction results for the various compositions of the BSTO composites are given in Table II. It should be noted that there are three different forms of Barium Aluminum Oxide listed within the table.

In agreement with EDX, the results reveal that when alumina is added to BSTO in small amounts, < 20 wt%, a second phase of Barium Aluminum Titanate, $Ba_3Al_{10}TiO_{20}$, is formed. In compositions having between 20 and 40 wt% alumina another phase of Barium Aluminum Titanate forms ie. $BaAl_6TiO_{12}$ In this composition range we are also seeing traces of Barium Aluminum Oxide, $BaAl_{13.2}O_{20.8}$. By the time the composition reaches 60 wt% alumina no Barium Aluminum Titanate phases are detected. Only faint traces of BSTO are discernible at this composition. At 60 wt% alumina it was not possible to discern which phase was most prevalent or even if all three phases were present. At 80 wt% alumina a specific phase of Barium Aluminum Oxide still could not be identified, but definite Al_2O_3 peaks became apparent. Pure alumina provided an expected diffraction pattern.

The results for the BSTO-Oxide II composites are completely different. The results show that initially oxide II appears to be absorbed into the BSTO lattice structure. At compositions from 5-50 wt% oxide II, BSTO is the dominant pattern, but at 60 wt%, oxide II becomes dominant. It is also interesting to note that no second phase materials were detected at any of the compositions for this composite. Similar results were observed for the BSTO-Oxide III composites. The only variation for the latter is that traces of oxide III are apparent even with only a 1 wt% addition.

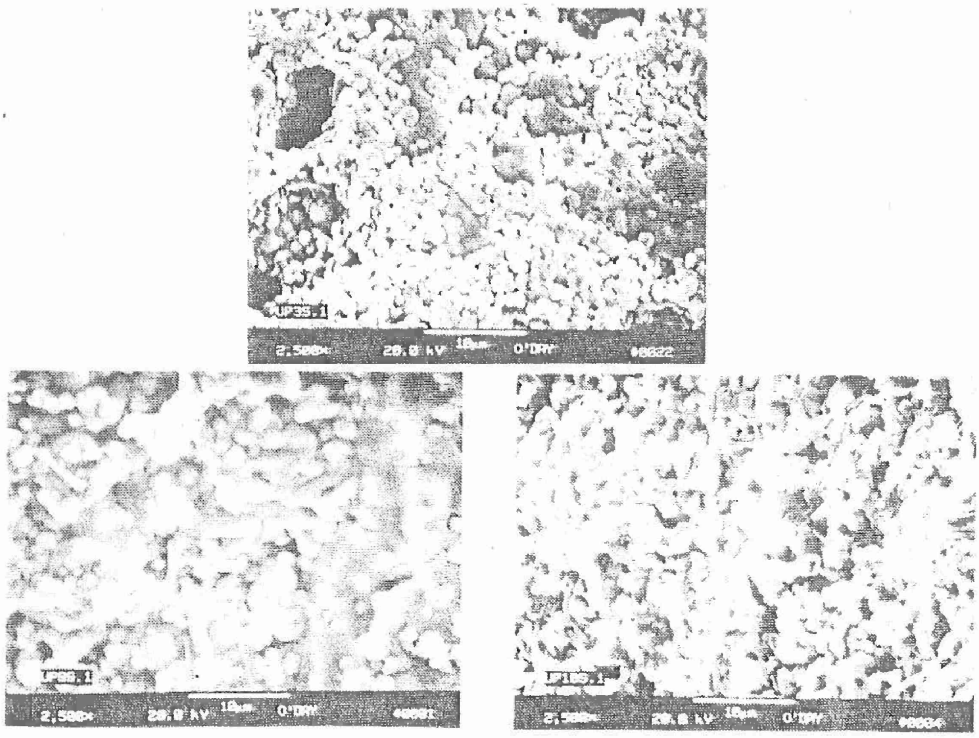

FIGURE 1 (a) SEM micrograph of BSTO-10 wt% Alumina bulk ceramic composite microstructure, (b) SEM micrograph of BSTO-35 wt% Alumina bulk ceramic composite microstructure, (c) SEM micrograph of BSTO-60 wt % Alumina bulk ceramic composite microstructure.

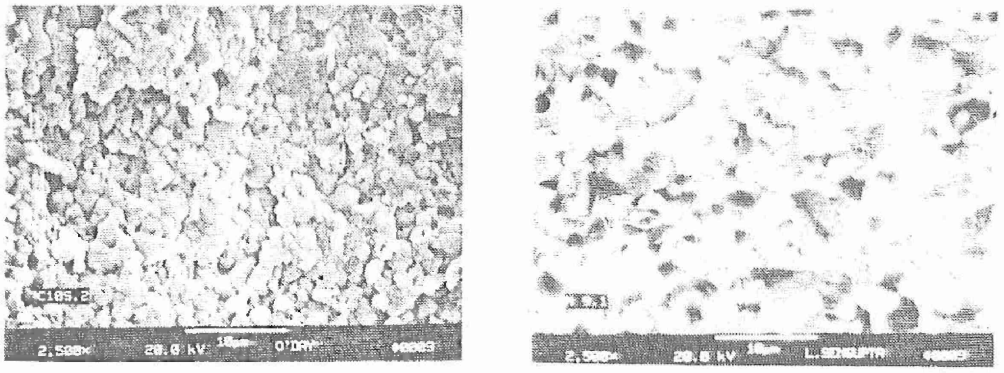

FIGURE 2 (a) SEM micrograph of BSTO-40 wt% Oxide II bulk ceramic composite microstructure, (b) SEM micrograph of BSTO-40 wt% Oxide III bulk ceramic composite microstructure.

TABLE II X-Ray Diffraction Results.

BSTO-Alumina

Oxide Content	*Detected Phases*
pure BSTO	$Ba_{.6}Sr_{.4}TiO_3$ pattern
1 wt% Al_2O_3	BSTO and $Ba_3Al_{10}TiO_{20}$
5 wt% Al_2O_3	BSTO and $Ba_3Al_{10}TiO_{20}$
10 wt% Al_2O_3	BSTO and $Ba_3Al_{10}TiO_{20}$
15 wt% Al_2O_3	BSTO and $Ba_3Al_{10}TiO_{20}$
20 wt% Al_2O_3	BSTO, $Ba_3Al_{10}TiO_{20}$ and $BaAl_{13.2}O_{20.8}$
25 wt% Al_2O_3	BSTO, $Ba_3Al_{10}TiO_{20}$, $BaAl_6TiO_{12}$ and $BaAl_{13.2}O_{20.8}$
30 wt% Al_2O_3	$Ba_3Al_{10}TiO_{20}$, $BaAl_6TiO_{12}$, BSTO and $BaAl_{13.2}O_{20.8}$
35 wt% Al_2O_3	$Ba_3Al_{10}TiO_{20}$, $BaAl_6TiO_{12}$, BSTO and $BaAl_{13.2}O_{20.8}$
40 wt% Al_2O_3	$Ba_3Al_{10}TiO_{20}$, $BaAl_6TiO_{12}$, BSTO and $BaAl_{13.2}O_{20.8}$
60 wt% Al_2O_3	Barium Aluminum Oxide (phase unknown) and BSTO
80 wt% Al_2O_3	Barium Aluminum Oxide (phase unknown) and Al_2O_3
pure Al_2O_3	Al_2O_3 pattern

3.3 Electronic Properties

The results for the electronic properties of the BSTO-Alumina composites are shown in Table III. In this and subsequent tables there are a few tunability data points missing due to either shorting caused by application of high voltages to poorly constructed electroding or because oxide additions > 60 wt% exhibit virtually no tunability. The dielectric constant of the specimens is quickly reduced for compositions up to 35 wt% alumina at which point the rate of reduction in the dielectric constant is diminished. The dielectric loss, tan δ, reported here for all specimens includes the loss caused by the metal contact, improved metallization for these materials will definitely result in loss tan $\delta < 0.01$. The % tunability of the specimens could be increased with an increase in applied electric field and by using thinner specimens. Even so, the tunability of the composites is maintained at reasonable levels (>10%) up to 20 wt% alumina at which time the tunability decreases rapidly. A graph of the Tunability versus Applied Field is shown in Fig. 3. The inset shows the Dielectric Constant of these compositions versus Tunability at an electric field of 0.7 V/μm.

Table IV contains the electronic data for the BSTO-Oxide II ceramic composites. As shown in Table IV the loss tangent of the materials are relatively low (<0.02). It appears that as the dielectric constant decreased the loss was lowered. The dielectric constant of the composites decreases with the addition of oxide II. The semi-log plot of the dielectric constants of the BSTO-Alumina composites, the BSTO-Oxide II composites and the BSTO-Oxide III composites is shown in Fig. 4. As shown in Fig. 4, the rate of reduction is similar for both composites for compositions < 20 wt%. However, between 20 wt% - 50 wt% the rate of reduction in the dielectric constant is less than that of the BSTO-Alumina composites. The decrease in the dielectric constant for the two sets of composites is again similar from 60 wt%-100 wt% additive content. However, the magnitude of the dielectric constant for all of theBSTO-Alumina composites is less than that of the BSTO-Oxide II and BSTO-Oxide III composites. This may be due to the formation of the second phases in the BSTO-Alumina composites.

The Tunability (%) versus Applied Electric Field for several compositions of BSTO-Oxide II composites is shown in Fig. 5. The inset represents the Dielectric Constant of these compositions versus Tunability (%) at an electric field of 0.7 V/μm. It is apparent that the tunability decreases for compositions less than 30 wt% oxide II. For additive contents >25 wt% and at similar electric fields, the tunability of the BSTO-Oxide II composites is greater than that of the BSTO-Alumina composites. This may again be due to the formation of second phases in the BSTO-Alumina composites, creating additional non-ferroelectric phases which inhibit tuning in the material.

The electronic data for the BSTO-Oxide III composites is shown in Table V. Similar trends were noticed for these composites with the exception of having lower losses in the other two composites. As shown in Fig. 6, the loss tangent of the composites are extremely low for most all compositions (decreases slightly with an increase in oxide III). These formulations could therefore be used at much higher operating frequencies, i.e., at millimeter wave range, @ 77 GHz. As shown in Fig. 4, the other electronic properties are similar to BSTO-Oxide II, except for the fact that the dielectric constants are even higher for these compositions in the range 15-60 wt%.

TABLE III Electronic Properties of BSTO (Ba = .6) and Alumina Ceramic Composites.

Alumina Content (wt %)	*Dielectric Constant*	*Loss Tangent*	*% Tunability*	*Electric Field (V/μm)*
0.0	3299.08	0.0195	19.91	0.73
1.0	2606.97	0.0122	22.50	0.76
5.0	1260.53	0.0630*	13.88	0.67
10.0	426.74	0.0163	4.79	0.39
15.0	269.25	0.0145	5.72	0.87
20.0	186.01	0.0181	3.58	0.48
25.0	83.07	0.0120		
30.0	53.43	0.0135	5.13	2.21
35.0	27.74	0.0029	0.51	0.83
40.0	25.62	0.1616*		
60.0	16.58	0.0009	0.01	0.60
80.0	12.70	0.0016		
100.0	8.37	0.0036		

* samples had poor contacts

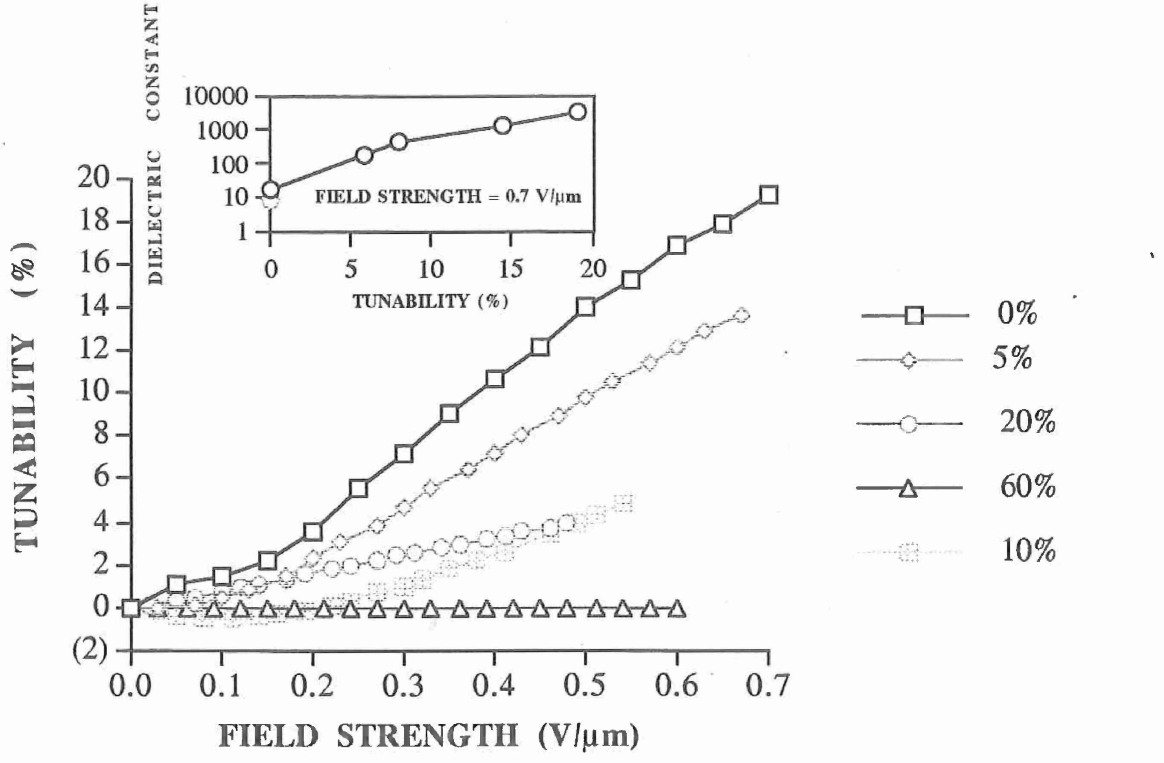

FIGURE 3 Tunability (%) versus Applied Electric Field (V/μm) for BSTO-Alumina composites (inset shows the Dielectric Constant versus Tunability (%) at an electric field of 0.7 V/μm).

TABLE IV Electronic Properties of BSTO-Oxide II Ceramic Composites

Oxide II Content (wt %)	*Dielectric Constant*	*Loss Tangent*	*% Tunability*	*Electric Field (V/μm)*
0.0	3299.08	0.0195	19.91	0.73
1.0	2696.77	0.0042	46.01	2.72
5.0	2047.00	0.0138	12.70	0.76
10.0	1166.93	0.0111	7.68	0.68
15.0	413.05	0.0159	5.07	1.11
20.0	399.39	0.0152	5.39	0.76
25.0	273.96	0.0240	6.02	1.02
30.0	233.47	0.0098	1.21	0.73
35.0	183.33	0.0091	5.87	0.95
40.0	162.26	0.0095	0.70	0.71
50.0	92.73	0.0071	1.67	1.12
60.0	69.80	0.0098		
80.0	17.31	0.0056		
100.0	15.98	0.0018	0.05	0.27

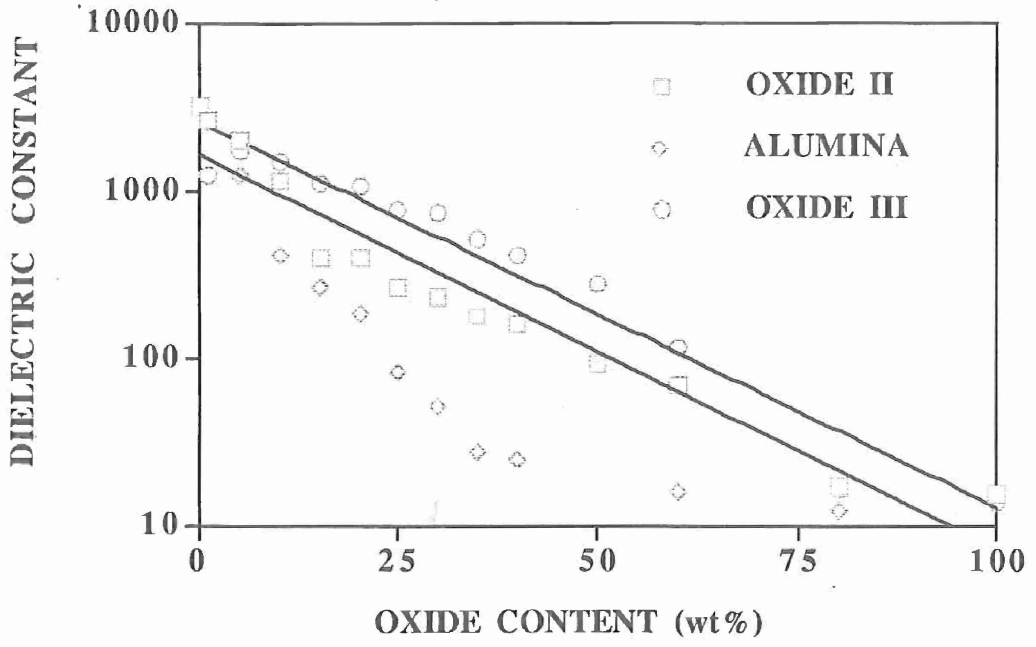

FIGURE 4 Semi-log plot of the Dielectric Constant versus Oxide Content (wt%) for, BSTO Oxide II, BSTO-Alumina and BSTO-Oxide III composites. (The lines shown depict the best logarithmic fit to the data.)

The tunability decreases slowly with increase in oxide III content and the compositions exhibit high tunabilities (>10%) up to 60 wt% oxide III which was not the case for the other composites.

3.4 Electroding / Encapsulation Results

In order to determine the metallization and packaging which produces the lowest loss tangents in the materials, we have investigated the use of screen printed fired-on external electroding (terminations) and we have also performed a cursory study on the effect of polymeric encapsulation on the specimens. To be self-consistent and to be within the application specifications for many antenna systems, the specimens chosen for this study were BSTO-Alumina (20wt%), BSTO-Oxide II (20 wt%) and BSTO-Oxide III (20 wt%). A description of the external electrodes used in this study is given in Table VI[3]. The electroding materials are manufactured by Ferro Corp., Electronic Materials Division, Santa Barbara, CA.

The BSTO-Alumina (20 wt%) composites showed an increase in the measured loss tangents when fired-on electrodes were used. The cause for this increase is currently under investigation. The results for the silver painted specimens are shown in Table VII. The data includes unencapsulated specimens with no wires, unencapsulated specimens with wires (attached with high purity silver epoxy), and wired specimens

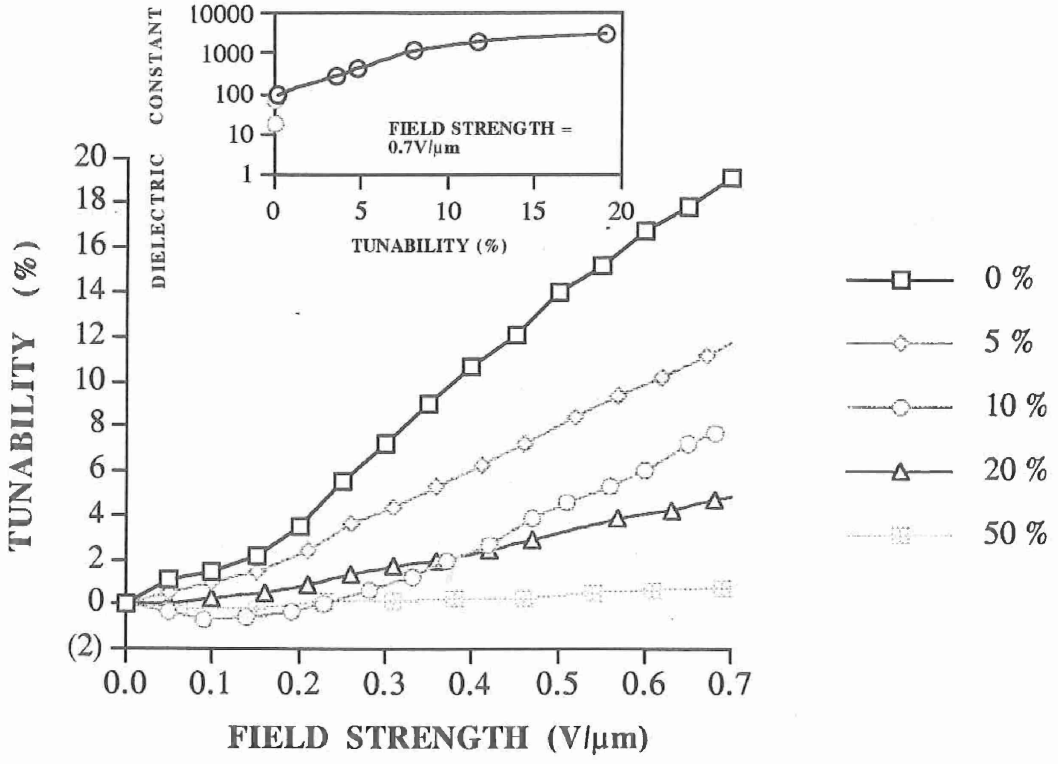

FIGURE 5 Tunability (%) versus Applied Electric Field (V/μm) for BSTO-Oxide II Composites (inset shows the Dielectric Constant versus Tunability (%) at an electric field of 0.7 V/μm).

TABLE V Electronic Properties of BSTO-Oxide III Ceramic Composites.

Oxide III Content (wt %)	*Dielectric Constant*	*Loss Tangent*	*% Tunability*	*Electric Field (V/μm)*
0.0	3299.08	0.0195	19.91	0.73
1.0	1276.21	0.0015	16.07	2.32
5.0	1770.42	0.0014		
10.0	1509.19	0.0018		
15.0	1146.79	0.0011	7.270	1.91
20.0	1079.21	0.0009	15.95	2.33
25.0	783.17	0.0007	17.46	2.45
30.0	750.93	0.0008	9.353	1.62
35.0	532.49	0.0006	18.00	2.07
40.0	416.40	0.0009	19.81	2.53
50.0	280.75	0.0117*	9.550	2.14
60.0	117.67	0.0006	11.08	2.70
80.0	17.00	0.0008	0.61	1.72
100.0	13.96	0.0009		

* samples had poor contacts

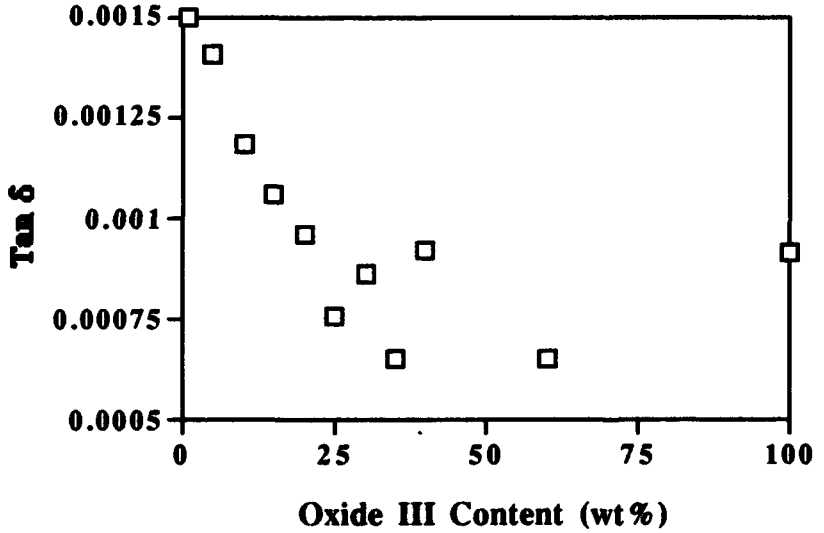

FIGURE 6 Loss Tangent versus Oxide III Content (wt %) for BSTO-Oxide III composites.

encapsulated with polyester resin. The loss is improved when leads are attached to the specimens due to improved contact.

The BSTO-Oxide II composites showed a drastic increase in the loss tangent for specimens which had fired-on electroding. The mechanism for this increase is also being investigated. Table VIII contains the dielectric constant and loss tangent for BSTO-Oxide II (20 wt%) composites which were not wired, wired and were encapsulated with polyester resin. Again, the loss is improved when leads are attached to the specimens.

The results for the dielectric constant and the loss tangent for the BSTO-Oxide III (20wt%) composites are shown in Table IX. For the samples which have fired-on electroding the wires were attached with 2% silver, 62% tin and 36% lead solder. The temperature of the solder was maintained at 215 +/- 5 ^{0}C, which controls the reaction rate between the fired-on electroding and the solder and therefore assures good adhesion. As shown in Table IX, the dielectric constant of the specimens are self-consistent. The loss tangents are about the same for all of the fired-on electrodes and they are lower than those obtained with silver paint for these composites. The loss is further decreased by attaching leads. This approaches the lowest loss measurement capability of the HP bridge (which may result in pseudo-negative values for some specimens). The dielectric constant appears to have increased for the specimens which have been soldered probably due to the inductance of the metallic/solder interface and variations in thickness seem to strongly influence the consistency of the results.

TABLE VI External Electroding[3].

Product No.	*Description*
3309	Fritted Silver; SnPb solderable
T2026	Standard Silver. SnPb solderable sold to PZT manufacturers
T2076	Compatible with various titanate formulations. Good adhesion
T2073	Platable termination for Barium Titanate
T2075	Platable and solderable. Termination for alumina and ferrite bodies.

TABLE VII Electroding Study of BSTO (w/20wt% Alumina) Samples.

Sample Ink #: Silver Paint	***Dielectric Constant*** Air Dried	***Loss Tangent @ 1MHz***
without wires		
BAL16	104.65	.0058460
BAL17	101.67	.0052430
BAL18	110.03	.0056130
with wires		
BAL16	107.81	.0044740
BAL17	102.29	.0047330
with encapsulant and wires		
BAL-17-polyester	105.40	.0048850

TABLE VIII Electroding Study of BSTO (w/20wt% Oxide II) Samples.

Sample Ink #: Silver Paint	***Dielectric Constant*** Air Dried	***Loss Tangent***	
without wires		**@ 1KHz**	
OX216	346.33	.043439	
OX217	379.75	.049499	
OX218	364.08	.049600	
with wires		@ 1KHz	@1 MHz
OX216	319.97	.025772	.018506
OX217	343.72	.027378	.014754
with encapsulant and wires			
OX2-17-polyester	254.69	.032847	.022930

The results for the encapsulation experiments are also shown in Table IX. The three encapsulants chosen were acrylic (conformal coating), polyester resin, and polyurethane (air-dry). The data indicate that the acrylic coating produces the largest effect on the electronic properties (decrease in dielectric constant and increase in the loss tangent) whereas the polyester has moderate changes in the electrical behavior of the materials. The polyurethane showed the least change in the properties and therefore this encapsulant appears to be the best candidate. Although, lower loss polymers, such as styrene, will be investigated in the near future and environmental (humidity) studies have not yet been performed.

TABLE IX Electroding Study of BSTO (w/20wt% Oxide III) Samples.

Sample	*Dielectric Constant*	*Loss Tangent @ 1MHz*
Ink #: 3309	**Firing Temperature:** 850 C	
without wires		
OX31	857.32	.0012550
OX32	886.76	.0004800
OX33	877.55	.0007320
with wires		
OX31	921.51	.0020380
OX32	916.63	.0026570
OX33	940.18	.0015210
with encapsulants		
OX31-acrylic	741.42	.0100670
OX32-polyurethane	899.25	.0006250
OX33-polyester	859.30	.0074740
Ink#: T2075	**Firing Temperature:** 500 C	
without wires		
OX34	895.21	.0007950
OX35	868.50	.0005060
OX36	867.88	.0003670
with wires		
OX34	979.70	.0013510
OX35	1012.33	.0003490
OX36	827.92	.0019000
with encapsulants		
OX34-acrylic	865.96	.0105490
OX35-polyester	914.67	-.1106180
OX36-poyurtethane	812.01	.0005150
Ink#: T2076	**Firing Temperature:** 600 C	
without wires		
OX37	863.38	.0020610
OX38	858.28	.0010720
OX39	881.93	.0011390
with wires		
OX37		
OX38	886.19	-.0017690
OX39	944.75	-.0008560
with encapsulants		
OX37-acrylic	894.97	.0018030
OX38-polyester	811.57	.0055840
OX39		

Sample	*Dielectric Constant*	*Loss Tangent @ 1MHz*
Ink#: T2026	**Firing Temperature:** 760 C	
without wires		
OX310	852.13	.0004020
OX311	881.99	.0002990
OX312	849.63	.0003260
with wires		
OX310	941.02	-.0017690
OX311	1010.07	-.0008560
OX312	931.99	-.0002650
with encapsulants		
OX310-polyester	898.12	-.0006630
OX311-polyurethane	949.13	.0003810
OX312-acrylic	949.65	-.0000320
Ink#: T2073	**Firing Temperature:** 850 C	
without wires		
OX313	872.78	.0003830
OX314	860.50	.0004570
OX315	873.77	.0005380
with wires		
OX313		
OX314	948.82	.0000550
OX315	963.85	.0000430
with encapsulants		
OX313-acrylic	986.01	.0000240
OX314-polyester	932.51	-.0002210
OX315-polyurethane	944.98	-.0000550
Ink#: Silver Paint	**Air Dried**	
without wires		
OX316	817.47	.0040370
OX317	809.62	.0052190
OX318	806.40	.0054000
with wires		
OX316	723.13	.0031750
OX317	685.10	.0044900
OX318	963.85	.0038760
with encapsulants		
OX316-acrylic		
OX317-polyester	669.78	.0050280
OX318-polyurethane		

4. CONCLUSIONS

Composites of BSTO and non-ferroelectric oxide ceramics have been fabricated and characterized. The composites have all demonstrated adjustable electronic properties. The dielectric constant of the BSTO-Alumina composites decreases faster than the BSTO-Oxide II and the BSTO-Oxide III composites from 20-50 wt% alumina content and is related to the formation of multiple secondary phases in this composition range for the BSTO-Alumina composites. The BSTO-Oxide III composites exhibited the lowest dielectric loss (<0.001) and highest dielectric constants in the composition range from 15-60 wt% oxide content. The BSTO-Alumina and BSTO-Oxide II composites did not show a decrease (as compared to silver paint) in the loss tangents. The BSTO-Oxide III specimens showed a drastic decrease in the loss tangents for specimens with fired-on electrodes. The attachment of leads improves the dielectric loss for all of the composites. The polyurethane encapsulant did not change the electronic properties of the BSTO-Oxide III composites.

5. ACKNOWLEDGMENTS

The authors would like to thank Philip Wong, ARL-MD, for his contributions to the SEM and EDX work in this paper. Also, the assistance of Daniel Snoha and Kyu Cho, ARL-MD, with "all" of the X-ray diffraction data is greatly appreciated.

6. REFERENCE LIST

1. R.W. Babbitt, T.E. Koscica, and W.E. Drach, "Planar Microwave Electro-Optic Phase Shifters," Microwave Journal **35** [6], p. 63-79 (1992).
2. A.H. Scott and H.L. Curtis, "Edge Correction and Determination of Dielectric Constant," J. of Res., UNBAA, Nat. Bureau of Standards, **22**, 747-745 (1939).
3. Ferro Corp., "Ferro A6 LTCC Materials Processing Guidelines" (1993).

DISTRIBUTION LIST

No. of Copies	To
1	Office of the Under Secretary of Defense for Research and Engineering, The Pentagon, Washington, DC 20301
	Director, U.S. Army Research Laboratory, 2800 Powder Mill Road, Adelphi, MD 20783-1197
1	ATTN: AMSRL-OP-SD-TP, Technical Publishing Branch
1	AMSRL-OP-SD-TM, Records Management Administrator
	Commander, Defense Technical Information Center, Cameron Station, Building 5, 5010 Duke Street, Alexandria, VA 23304-6145
2	ATTN: DTIC-FDAC
1	MIA/CINDAS, Purdue University, 2595 Yeager Road, West Lafayette, IN 47905
	Commander, Army Research Office, P.O. Box 12211, Research Triangle Park, NC 27709-2211
1	ATTN: Information Processing Office
	Commander, U.S. Army Materiel Command, 5001 Eisenhower Avenue, Alexandria, VA 22333
1	ATTN: AMCSCI
	Commander, U.S. Army Materiel Systems Analysis Activity, Aberdeen Proving Ground, MD 21005
1	ATTN: AMXSY-MP, H. Cohen
	Commander, U.S. Army Missile Command, Redstone Arsenal, AL 35809
1	ATTN: AMSMI-RD-CS-R/Doc
	Commander, U.S. Army Armament, Munitions and Chemical Command, Dover, NJ 07801
2	ATTN: Technical Library
	Commander, U.S. Army Natick Research, Development and Engineering Center, Natick, MA 01760-5010
1	ATTN: DFAS-IN-EM-TL, Technical Library
	Commander, U.S. Army Satellite Communications Agency, Fort Monmouth, NJ 07703
1	ATTN: Technical Document Center
	Commander, U.S. Army Tank-Automotive Command, Warren, MI 48397-5000
1	ATTN: AMSTA-ZSK
1	AMSTA-TSL, Technical Library
	Commander, White Sands Missile Range, NM 88002
1	ATTN: STEWS-WS-VT
	President, Airborne, Electronics and Special Warfare Board, Fort Bragg, NC 28307
1	ATTN: Library
	Director, U.S. Army Research Laboratory, Weapons Technology, Aberdeen Proving Ground, MD 21005-5066
1	ATTN: AMSRL-WT

No. of Copies	To
	Commander, Dugway Proving Ground, UT 84022
1	ATTN: Technical Library, Technical Information Division
	Commander, U.S. Army Research Laboratory, 2800 Powder Mill Road, Adelphi, MD 20783
1	ATTN: AMSRL-SS
	Director, Benet Weapons Laboratory, LCWSL, USA AMCCOM, Watervliet, NY 12189
1	ATTN: AMSMC-LCB-TL
1	AMSMC-LCB-R
1	AMSMC-LCB-RM
1	AMSMC-LCB-RP
	Commander, U.S. Army Foreign Science and Technology Center, 220 7th Street, N.E., Charlottesville, VA 22901-5396
3	ATTN: AIFRTC, Applied Technologies Branch, Gerald Schlesinger
	Commander, U.S. Army Aeromedical Research Unit, P.O. Box 577, Fort Rucker, AL 36360
1	ATTN: Technical Library
	U.S. Army Aviation Training Library, Fort Rucker, AL 36360
1	ATTN: Building 5906-5907
	Commander, U.S. Army Agency for Aviation Safety, Fort Rucker, AL 36362
1	ATTN: Technical Library
	Commander, Clarke Engineer School Library, 3202 Nebraska Ave., N, Fort Leonard Wood, MO 65473-5000
1	ATTN: Library
	Commander, U.S. Army Engineer Waterways Experiment Station, P.O. Box 631, Vicksburg, MS 39180
1	ATTN: Research Center Library
	Commandant, U.S. Army Quartermaster School, Fort Lee, VA 23801
1	ATTN: Quartermaster School Library
	Naval Research Laboratory, Washington, DC 20375
2	ATTN: Dr. G. R. Yoder - Code 6384
	Chief of Naval Research, Arlington, VA 22217
1	ATTN: Code 471
	Commander, U.S. Air Force Wright Research & Development Center, Wright-Patterson Air Force Base, OH 45433-6523
1	ATTN: WRDC/MLLP, M. Forney, Jr.
1	WRDC/MLBC, Mr. Stanley Schulman
	U.S. Department of Commerce, National Institute of Standards and Technology, Gaithersburg, MD 20899
1	ATTN: Stephen M. Hsu, Chief, Ceramics Division, Institute for Materials Science and Engineering

No. of Copies	To
1	Committee on Marine Structures, Marine Board, National Research Council, 2101 Constitution Avenue, N.W., Washington, DC 20418
1	Materials Sciences Corporation, Suite 250, 500 Office Center Drive, Fort Washington, PA 19034
1	Charles Stark Draper Laboratory, 555 Technology Square, Cambridge, MA 02139
	Wyman-Gordon Company, P.O. Box 8001, North Grafton, MA 01536-8001
1	ATTN: Technical Library
	General Dynamics, Convair Aerospace Division, P.O. Box 748, Fort Worth, TX 76101
1	ATTN: Mfg. Engineering Technical Library
	Plastics Technical Evaluation Center, PLASTEC, ARDEC, Bldg. 355N, Picatinny Arsenal, NJ 07806-5000
1	ATTN: Harry Pebly
1	Department of the Army, Aerostructures Directorate, MS-266, U.S. Army Aviation R&T Activity - AVSCOM, Langley Research Center, Hampton, VA 23665-5225
1	NASA - Langley Research Center, Hampton, VA 23665-5225
	U.S. Army Vehicle Propulsion Directorate, NASA Lewis Research Center, 2100 Brookpark Road, Cleveland, OH 44135-3191
1	ATTN: AMSRL-VP
	Director, Defense Intelligence Agency, Washington, DC 20340-6053
1	ATTN: ODT-5A (Mr. Frank Jaeger)
	U.S. Army Communications and Electronics Command, Fort Monmouth, NJ 07703
1	ATTN: Technical Library
	U.S. Army Communications and Electronics Command, Intelligence and Electronic Warfare Center, Fort Monmouth, NJ 07703-5211
1	ATTN: Frank Elmer, AMSEL-RD-IEW-TAE-M
	U.S. Army Research Laboratory, Electronic Power Sources Directorate, Fort Monmouth, NJ 07703
1	ATTN: AMSRL-EP-M, W. C. Drach
1	AMSRL-EP-M, T. E. Koscica
1	AMSRL-EP-M, R. W. Babbit
	Director, U.S. Army Research Laboratory, Watertown, MA 02172-0001
2	ATTN: AMSRL-OP-WT-IS, Technical Library
25	Authors